

The Possibility of Modeling the Very High Energy Afterglow of GRB 221009A in a Wind Environment

JIA REN,^{1,2} YUN WANG,^{3,4} LU-LU ZHANG,⁵ AND ZI-GAO DAI^{4,1}

¹School of Astronomy and Space Science, Nanjing University, Nanjing 210023, China

²Key Laboratory of Modern Astronomy and Astrophysics (Nanjing University), Ministry of Education, Nanjing 210023, China

³Key Laboratory of Dark Matter and Space Astronomy, Purple Mountain Observatory, Chinese Academy of Sciences, Nanjing 210034, China

⁴Department of Astronomy, School of Physical Sciences, University of Science and Technology of China, Hefei 230026, China

⁵Guangxi Key Laboratory for Relativistic Astrophysics, School of Physical Science and Technology, Guangxi University, Nanning 530004, China

Submitted to ApJ

ABSTRACT

In this paper, we model the dynamics and radiation physics of the rarity event GRB 221009A afterglow in detail. By introducing a top-hat jet that propagates in an environment dominated by stellar winds, we explain the publicly available observations of afterglow associated with GRB 221009A over the first week. It is predicted that GRB 221009A emits a luminous very high energy (VHE) afterglow based on the synchrotron self-Compton (SSC) process in our model. We show the broadband spectral energy distribution (SED) analysis results of GRB 221009A, and find that the SSC radiation component of GRB 221009A is very bright in the 0.1 – 10 TeV band. The integrated SED shows that the SSC emission in the TeV band has significantly higher than the detection sensitivity of LHASSO, MAGIC and CTA. However, since the release of further observations, deviations from the standard wind environment model gradually show up in data. For example, the late-time multiband afterglow cannot be consistently explained under the standard wind environment scenario. It may be necessary to consider modeling with a structured jet with complex geometry or a partial revision of the standard model. Furthermore, we find that the inclusion of GeV observations could break the degeneracy between model parameters, highlighting the significance of high-energy observations in determining accurate parameters for GRB afterglows.

Keywords: Gamma-ray bursts (629); High energy astrophysics (739)

1. INTRODUCTION

On 2022 October 9 at 13:16:59 UT, the *Fermi* Gamma-Ray Burst Monitor (GBM) triggered long duration gamma-ray burst GRB 221009A (Veres et al. 2022). Not too late, at 14:10:17 UT, The *Swift* Burst Alert Telescope (BAT) triggered GRB 221009A, aka Swift J1913.1+1946 (Dichiara et al. 2022). The *Fermi* Large Area Telescope (LAT) detected high-energy

emission from GRB 221009A at 14:17:05.99 (Bissaldi et al. 2022a), and the high energy photon observed by *Fermi*/LAT reaches 99.3 GeV (Pillera et al. 2022), even 397.7 GeV (Xia et al. 2022). The *Swift* X-ray Telescope (XRT) have fruitful follow up observations (Bissaldi et al. 2022b). GRB 221009A is extraordinary bright with isotropic prompt emission energy $E_{\gamma,\text{iso}} \simeq 1.5 \times 10^{55}$ erg (An et al. 2023; Yang et al. 2023) with redshift $z = 0.151$ (de Ugarte Postigo et al. 2022b; Castro-Tirado et al. 2022; Malesani et al. 2023). Very energetic GRBs at such close distances are estimated to occur only once in a century (Atteia 2022) or even ten thousand years (Burns et al. 2023), and it is possible to detect very high energy (VHE) photons (Xue et al. 2009). As expected, China’s Large High Altitude

Corresponding author: Jia Ren
 jia@smail.nju.edu.cn

Corresponding author: Zi-Gao Dai
 daizg@ustc.edu.cn

Air Shower Observatory (LHAASO) recorded at least tens of thousands of photon signals in the VHE region above 100 GeV, including photons with energy greater than 10 TeV (Huang et al. 2022), which can give the finest measurement of the lightcurve in the highest energy band of GRBs.

In recent years, several long GRBs have been successfully observed corresponding VHE afterglows. Long GRBs with the same VHE afterglows as GRB 221009A, including GRBs 180720B, 190114C, 190829A, 201015A, and 201216C, have four orders of magnitude on $E_{\gamma,\text{iso}}$ from $\sim 10^{50}$ erg to $\sim 10^{54}$ erg. The VHE afterglow of GRB 180720B ($E_{\gamma,\text{iso}} = 6 \times 10^{53}$ erg at $z = 0.654$) were firstly detected with the High Energy Stereoscopic System (H.E.S.S.) in a confidence level of 5.3σ in the $0.1 - 0.4$ TeV band (Abdalla et al. 2019). Moreover, the VHE afterglow of GRB 190114C ($E_{\gamma,\text{iso}} = 3 \times 10^{53}$ erg at $z = 0.4245$) was convincingly detected with the Major Atmospheric Gamma Imaging Cerenkov (MAGIC) telescopes in the $0.3 - 1$ TeV band in a high confidence level of $> 50\sigma$ (MAGIC Collaboration et al. 2019). The TeV afterglow of nearby GRB 190829A was detected ($E_{\gamma,\text{iso}} = 2 \times 10^{50}$ erg at $z = 0.0785$) with H.E.S.S. in the $0.2 - 4$ TeV band with a confidence level of 21.7σ (H. E. S. S. Collaboration et al. 2021). The VHE afterglows of GRBs 201015A (> 140 GeV, 3.5σ , Suda et al. 2021) and 201216C (~ 100 GeV, 6σ , Fukami et al. 2021) were detected by the MAGIC telescopes also, but the data have not yet been released. These two bursts have prompt emission energy $E_{\gamma,\text{iso}} = 1.1 \times 10^{50}$ erg with the redshift $z = 0.423$ of GRB 201015A, and $E_{\gamma,\text{iso}} = 5.76 \times 10^{53}$ erg with the redshift $z = 1.1$ of GRB 201216C, respectively (Zhang et al. 2022, in preparation). Since the extragalactic background light (EBL) absorbs sub-TeV/TeV photons from high-redshift sources, the VHE afterglows of low-redshift GRBs should be easier to detect (e.g., Finke et al. 2010; Domínguez et al. 2011). Overall, it seems that both energetic and sub-energetic GRBs can accelerate the particles to an extremely high energy and produce the VHE afterglows (e.g. Hurley et al. 1994; Murase et al. 2006).

The new window opened on TeV emission of GRBs usher in a new era of GRB physics at extremely high energy. The VHE afterglows of GRBs are generally believed to be attributed to synchrotron, synchrotron self-Compton (SSC), and/or external inverse-Compton (EIC) radiations of the electrons accelerated in relativistic jets (e.g., Dermer et al. 2000; Zhang & Mészáros 2001; Sari & Esin 2001; He et al. 2009; MAGIC Collaboration et al. 2019; Acciari et al. 2021; H. E. S. S. Collaboration et al. 2021; Zhang et al. 2021; Zhang et al. 2021). Besides, the hadronic processes may also play

an important role (e.g., Sahu et al. 2022). To distinguishing between these components, accurate modeling of broadband spectral energy distributions (SEDs) is required. Thus, abundant and high-quality observations from radio to TeV at same timeslices for SEDs and continuously monitored multiband afterglow lightcurves will provide a powerful support for understanding the physics of GRB radiation (e.g., Wang et al. 2019; Zhang et al. 2020; Joshi & Razzaque 2021; Yamasaki & Piran 2022).

It is widely accepted that long GRBs can occur during the core collapse of stars. Accordingly, stars may have undergone a drastic material-loss process before finally collapsing, resulting in circumburst environments dominated by stellar winds (Dai & Lu 1998; Chevalier & Li 2000). Previous works have inferred that GRB 190114C maybe occur in stellar wind environment, but the other possibilities have not been ruled out (e.g., Asano et al. 2020; Joshi & Razzaque 2021). In this work, we find that the afterglow lightcurve and SED of GRB 221009A may support this occurrence. Although other possibilities cannot be ruled out, such as a structured jet, our work firstly provides a interpretation of the observations.

This paper is organized as follows. In Section 2, we briefly describe the analysis and collection of observational data. In Section 3, we introduce our model considerations in detail and present the results of model parameter inference. We summarize and discuss the significance of our results in Section 5. We take the cosmology parameters as $H_0 = 67.8$ km s $^{-1}$ Mpc $^{-1}$, and $\Omega_M = 0.308$ (Planck Collaboration et al. 2016).

2. MULTIWAVELENGTH OBSERVATION AND SPECTRAL ANALYSIS OF GRB 221009A

2.1. *Fermi*/LAT data analysis

Fermi/LAT is a pair conversion telescope covering a wide energy band (from 20 MeV to greater than 300 GeV, Atwood et al. 2009). We analyze the observation data of *Fermi*/LAT in the direction of GRB 221009A (RA = 288.282, Dec = 19.495, from Pillera et al. (2022) based on the standard procedure¹. Considering the duration and high-energy events of GRB 221009A (Xia et al. 2022), data were extracted with the energy range of 100 MeV to 1 TeV, using transient event class (ev-class=16) before 400 seconds and source event class (ev-class=128) after that, and the corresponding instrument response functions (IRFs) file are used in the unbinned likelihood analysis. We perform these analyses by using the `Fermi`tools package and use `make4FGLxml` from

¹ <https://fermi.gsfc.nasa.gov/ssc/data/analysis/scitools/>

user contributions² to generate initial model files. For bins with TS values < 9 , we use the `UpperLimits` tool to calculate the upper limit of flux. Considering possible pile-up effects (Omodei et al. 2022) and the caveats given by *Fermi*³, we ignore the LAT data of GBM trigger time (Veres et al. 2022) $T_0 - T_0 + 294$ seconds.

2.2. Other follow-up observations

We have collected follow-up observations that have been reported from GCN⁴ or ATel⁵. For the *Swift*/XRT observation data, we rebin the 0.3–10 keV light curve based on the counts per bin (PC=600, WT=200)⁶, from about 3300 seconds to 2.3 days after *Fermi*/GBM trigger. We take into account the information of the time-resolved spectrum into the converting count-rates to energy fluxes from the spectral evolution data given by the “burst analyzer” tool⁷ (see more details in Evans et al. 2007, 2009). And, the *Swift*/XRT spectrum in the different time slices we used are extracted by an online analysis tool⁸. We have collected the optical data (r, r', R and z -band, Hu et al. 2022; Belkin et al. 2022b; de Wet & Groot 2022; Brivio et al. 2022; Gregory et al. 2022; Kumar et al. 2022; Chen et al. 2022; Zheng et al. 2022; Kim et al. 2022; Groot et al. 2022; Belkin et al. 2022a; Watson et al. 2022; Strausbaugh & Cucchiara 2022; Vinko et al. 2022; Zaznabin et al. 2022; Bikmaev et al. 2022a,b; Huber et al. 2022; Shrestha et al. 2022a,b; Brethauer et al. 2022) and radio data (frequencies around 1.5 GHz, 5 GHz, 15 GHz and 97.5 GHz, Bright et al. 2022; Farah et al. 2022; de Ugarte Postigo et al. 2022a; Rhodes et al. 2022; Laskar et al. 2022; Urata et al. 2022; Trushkin et al. 2022) for our model analysis. In addition, the High-Altitude Water Cherenkov Observatory (HAWC) has reported their observation result started from ~ 8 hours after the trigger time and lasted ~ 3.4 hours. Assuming a power law spectrum with photon index of -2.0 , they found no significant detection and proceeded to calculate the 95% upper limit on the flux at 1 TeV as 4.16×10^{-12} TeV cm 2 s $^{-1}$ (HAWC collaboration 2022).

2.3. Joint spectral analysis of X-ray and optical band

We have checked whether or not the host galaxy extinction exists at the optical band. The joint spectral

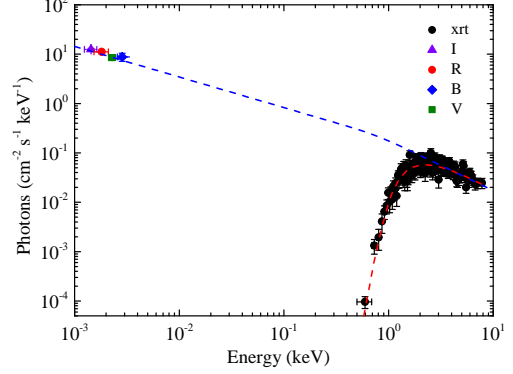


Figure 1. Joint optical-X-ray afterglow observed in the time interval of $[5.3 \sim 5.7] \times 10^4$ seconds of GRB 221009A along with our fit with a broken power-law function (the red dashed line). The optical data are extinction-corrected for our Galaxy. The H I absorption of our Galaxy is also considered in our spectral fit. The blue dashed line is plotted by using the model parameters of photon indices and break energy.

analysis of X-ray and optical afterglows at the timeslice from 5.3×10^4 to 5.7×10^4 seconds is using `XSPEC` (version 12.12.1) package. The above epoch including R, I, B, V bands and they are AB magnitude except for the B band (Gregory et al. 2022; Zheng et al. 2022). The Galactic extinctions of four bands are $A_R = 3.339$, $A_I = 2.317$, $A_V = 4.221$ and $A_B = 5.582$, respectively⁹. (Schlafly & Finkbeiner 2011). The Galactic H I column density $N_H^{\text{Gal}} = 5.36 \times 10^{21} \text{ cm}^{-2}$ at the GRB direction is fixed. The extinction curve of the host galaxy is taken as the same of Mike Way (MW) (Pei 1992) by setting $R_V = 3.08$. We find that the extinction value of the host galaxy with the absorption model is very small and negligible. Finally, we fit the joint spectrum of the X-ray-optical afterglow with a broken power-law model and the derived photon index are $\Gamma_{\text{O,X}}^1 = 1.62 \pm 0.17$ and $\Gamma_{\text{O,X}}^2 = 2.02 \pm 0.08$. The break energy is $E_{\text{break}} = (0.79 \pm 2.18)$ keV. The reduced χ^2 is $141.03/143 = 0.99$. The fitting result is shown in Figure 1. Currently, some works present results of the extinction values of GRB 221009A and find some significant influence from the host galaxy (e.g., Kann et al. 2023; Levan et al. 2023; Williams et al. 2023). Our results may differ due to the lack of UV band in the data we used, owing to the broken power-law spectral index differing from the prediction based on synchrotron radiation mechanism.

² <https://fermi.gsfc.nasa.gov/ssc/data/analysis/user/>

³ <https://fermi.gsfc.nasa.gov/ssc/data/analysis/grb221009a.html>

⁴ <https://gcn.gsfc.nasa.gov>

⁵ <https://www.astronomerstelegram.org>

⁶ https://www.swift.ac.uk/xrt_curves/

⁷ https://www.swift.ac.uk/burst_analyser/

⁸ https://www.swift.ac.uk/xrt_spectra/

⁹ <https://ned.ipac.caltech.edu/forms/calculator.html>

3. PHYSICAL IMPLICATION

3.1. Afterglow model Inference

We try to explain the multiband observations of GRB 221009A from radio to GeV band and infer the physical parameters through the afterglow model. The afterglow model is based on a Python-Fortran hybrid code **ASGARD** package we developed and can be modi-

fied for different physical considerations (e.g., Ren et al. 2020; Zhang et al. 2021). In this work, we consider the synchrotron radiation and SSC processes of electrons in the jet to generate realistic radiation behavior. We briefly describe the main numerical methods and model used as follows.

The dynamics of the external-forward shock of the jet described as (Nava et al. 2013; Zhang 2018),

$$\frac{d\Gamma}{dr} = -\frac{\Gamma(\Gamma^2 - 1)(\hat{\gamma}\Gamma - \hat{\gamma} + 1)\frac{dm}{dr}c^2 - (\hat{\gamma} - 1)\Gamma(\hat{\gamma}\Gamma^2 - \hat{\gamma} + 1)(3U/r)}{\Gamma^2[m_0 + m]c^2 + (\hat{\gamma}^2\Gamma^2 - \hat{\gamma}^2 + 3\hat{\gamma} - 2)U}, \quad (1)$$

$$\frac{dU}{dr} = (1 - \epsilon)(\Gamma - 1)c^2\frac{dm}{dr} - (\hat{\gamma} - 1)\left(\frac{3}{r} - \frac{1}{\Gamma}\frac{d\Gamma}{dr}\right)U, \quad (2)$$

where $dm/dr = n(r)m_p r^2$ with $n(r)$ being the particle density of circum-burst medium and m_p being the proton mass, and $\Gamma(r)$, $m(r)$, $U(r)$, and ϵ are the bulk Lorentz factor, the swept-up mass, the internal energy, and the radiation efficiency of electrons in the external-forward shock, respectively. The adiabatic index is $\hat{\gamma} \simeq (5 - 1.21937\zeta + 0.18203\zeta^2 - 0.96583\zeta^3 + 2.32513\zeta^4 - 2.39332\zeta^5 + 1.07136\zeta^6)/3$ with $\zeta \equiv \Theta/(0.24 + \Theta)$, $\Theta \simeq (\Gamma\beta/3)[\Gamma\beta + 1.07(\Gamma\beta)^2]/[1 + \Gamma\beta + 1.07(\Gamma\beta)^2]$, and $\beta = \sqrt{1 - 1/\Gamma^2}$ (Pe'er 2012). We have numerically solved equations (1) and (2) with the forth-order Runge-Kutta method. ϵ_e and ϵ_B are the equipartition factors for the energy in electrons and magnetic field in the shock, respectively. Then, the magnetic field behind the shock is $B' = [32\pi\epsilon_B n(r)]^{1/2}\Gamma c$, where ‘‘r’’ marks the co-moving frame of shock. The swept-in electrons by the shock are accelerated to a power-law distribution of Lorentz factor γ_e , i.e., $Q \propto \gamma_e^{-p}$ for $\gamma_{e,\min}' \leq \gamma_e \leq \gamma_{e,\max}'$, where $p (> 2)$ is the power-law index, $\gamma_{e,\min} = \epsilon_e(p-2)m_p\Gamma/[(p-1)m_e]$ (Sari et al. 1998), and $\gamma_{e,\max} = \sqrt{9m_e^2c^4/[8B'q_e^3(1+Y)]}$ with q_e being the electron charge (Kumar et al. 2012), where Y is the Compton parameter. Then, one can have $\epsilon = \epsilon_{\text{rad}}\epsilon_e$ with $\epsilon_{\text{rad}} = \min\{1, (\gamma_{e,\min}/\gamma_{e,c})^{(p-2)}\}$ (Sari & Esin 2001; Fan et al. 2008), where $\gamma_{e,c} = 6\pi m_e c / [\sigma_T \Gamma B'^2 t'(1+Y)]$ is the efficient cooling Lorentz factor of electrons with σ_T being the Thomson scattering cross section.

We denote the instantaneous electron spectrum as $dN_e/d\gamma'_e$, of which the evolution can be solved based on the continuity equation of electrons,

$$\frac{\partial}{\partial t'} \left(\frac{dN_e}{d\gamma'_e} \right) + \frac{\partial}{\partial \gamma'_e} \left[\dot{\gamma}'_{e,\text{tot}} \left(\frac{dN_e}{d\gamma'_e} \right) \right] = Q(\gamma'_e, t'), \quad (3)$$

We refer to Fan et al. (2008) for the way to solve this equation. We note that the Compton parameter $Y(\gamma'_e)$ has been solved based on the work of Fan & Piran

(2006). On the numerical method, we solve the continuity equation using a finite difference method of the third-order total-variation-diminishing Runge-Kutta method of time t' (TVD+RK3) and fifth-order weighted essentially non-oscillatory method of γ'_e (WENO5, Jiang & Shu 1996).

In the X-ray/optical/radio bands, the main radiation mechanism of the electrons in GRB jets is synchrotron radiation (Sari et al. 1998; Sari & Piran 1999). The spectral power of synchrotron radiation of $n'_e(r, \gamma'_e)$ at a given frequency ν' is

$$P'(\nu', r) = \frac{\sqrt{3}q_e^3 B'}{m_e c^2} \int_0^{\gamma'_{e,\max}} F\left(\frac{\nu'}{\nu'_c}\right) n'_e(r, \gamma'_e) d\gamma'_e, \quad (4)$$

where $F(x) = x \int_x^{+\infty} K_{5/3}(k) dk$ with $K_{5/3}(k)$ being the modified Bessel function of 5/3 order and $\nu'_c = 3q_e B' \gamma_e'^2 / (4\pi m_e c)$.

The emission of the SSC process is calculated based on the electron spectrum and seed photons from the synchrotron radiation (e.g., Geng et al. 2018; Huang 2022). We have numerically solved the Klein-Nishina effect and the $\gamma\gamma$ annihilation effects (e.g., Gould & Schréder 1967; Fan et al. 2008; Nakar et al. 2009; Murase et al. 2011; Geng et al. 2018).

We set the GRB jet as an on-axis-observed top-hat jet without considering the lateral expansion. The effect of the equal-arrival-time surface (EATS) is considered (e.g., Waxman 1997). We divide the radiation surface as small rings for the on-axis-observed jet. The intrinsic SEDs can be obtained from the integration over the EATS after considering the Doppler boosting effect. The EBL absorption effect is taken into account for calculating the observed high energy photons (Domínguez et al. 2011). By summing the flux from each ring observed at a same observer time, the total observed flux can be obtained.

3.2. Inference Results

Table 1. Multiband Fitting Results with the Forward Shock Model

GRB	$\log_{10}E_{k,\text{iso}}$ (erg)	$\log_{10}\Gamma_0$	p	$\log_{10}\epsilon_e$	$\log_{10}\epsilon_B$	$\log_{10}\theta_j$	$\log_{10}A_\star$
221009A	$54.83^{+0.10}_{-0.08}$	$2.28^{+0.02}_{-0.03}$	$2.60^{+0.03}_{-0.02}$	-0.69 ± 0.02	$-2.73^{+0.07}_{-0.10}$	$-1.61^{+0.06}_{-0.06}$	$-1.91^{+0.01}_{-0.01}$

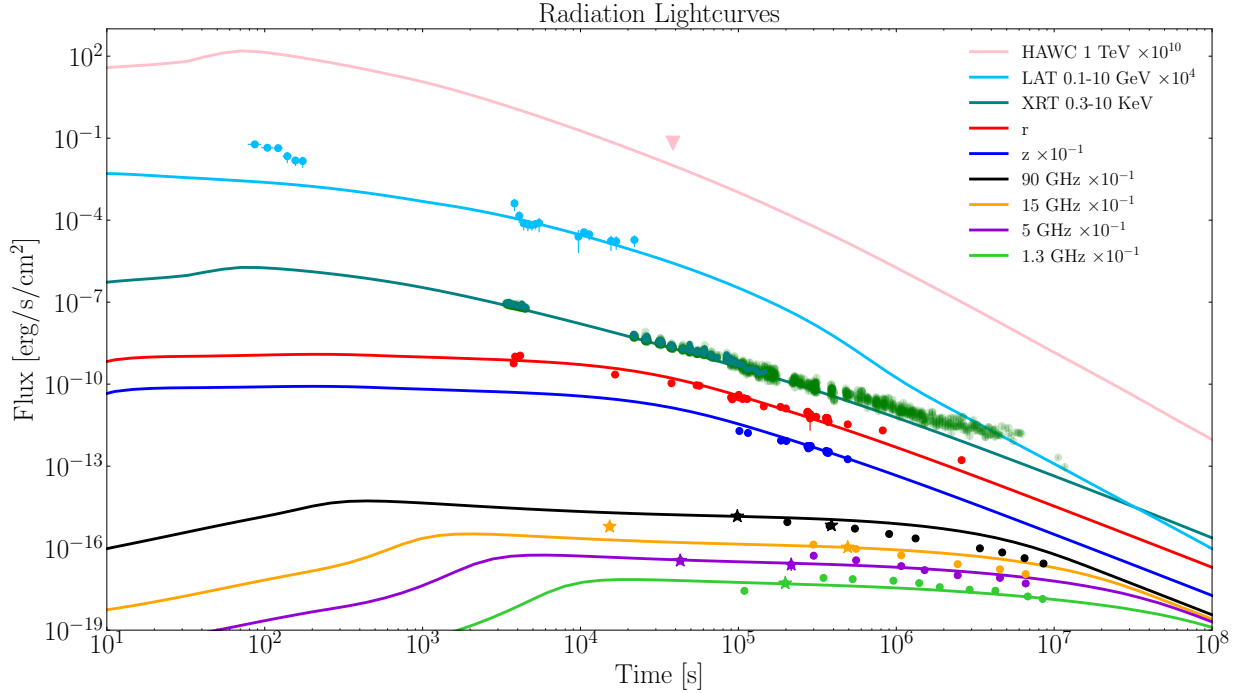


Figure 2. Multiband lightcurves from radio to TeV band plotted with our best fitting result. The jet generation time is set at $T_0 + 220$ s with T_0 being the trigger time of *Fermi*/GBM. The optical data have performed the Galactic extinction correction, and the light curve at 1 TeV has considered the EBL absorption. We show the HAWC 1 TeV upper limit at $T_0 + 8$ hours. We have added newly publicly available data released during the review process. For easy differentiation, the radio data used in our fitting are marked by stars, and the latest X-ray data are indicated by transparent circles. Although the optical and X-ray data suggest that model curves need to have a larger jet opening-angle, the different slopes between the X-ray and radio band data are systematic so that they cannot be explained by the standard stellar wind environment model.

We use the `emcee` Python package (Foreman-Mackey et al. 2013) to fit the lightcurves from radio to GeV bands and the spectra of *Swift*/XRT and *Fermi*/LAT (see Section 3.3). The parameter inference has been performed, including the isotropic kinetic energy $E_{k,\text{iso}}$, the electron energy fraction ϵ_e , the magnetic energy fraction ϵ_B , p , the initial bulk Lorentz factor Γ_0 , the half-opening angle of jet θ_j , and the wind parameter A_\star . Note that the number density of medium $n(r) = 3 \times 10^{35} A_\star r^{-2} \text{ cm}^{-3}$. Considering that the precursor radiation is observed when the GBM trigger, the energy of precursor is not sufficient to drive a powerful jet. Hence we set the generation time of an energetic jet as $\sim T_0 + 220$ s, which is the time of the main burst start. Furthermore, we have also considered the Galactic extinction in the r and z bands which

are $A_r = 3.52$ mag and $A_z = 1.95$ mag, respectively (Schlafly & Finkbeiner 2011). Additionally, extinction from host galaxy $E(B-V)_{\text{host}} = 0.185$ has chosen with $R_{V,\text{host}} = 2.93$ (SMC, Pei 1992; Kann et al. 2023).

We have examined the possibility of GRB 221009A that took place in a typical interstellar medium (ISM) environment. We find that for reasonable parameters the model curves of on-axis viewed top-hat jet are always higher than the observed data reported in radio bands, say, the radio observations strongly reject the ISM environment under this scenario. As a result, we find that the multiband afterglow of GRB 221009A can be explained by a relativistic jet propagating in the circumburst environment dominated by a stellar wind (Dai & Lu 1998). Our fitting results are shown in Figure 2.

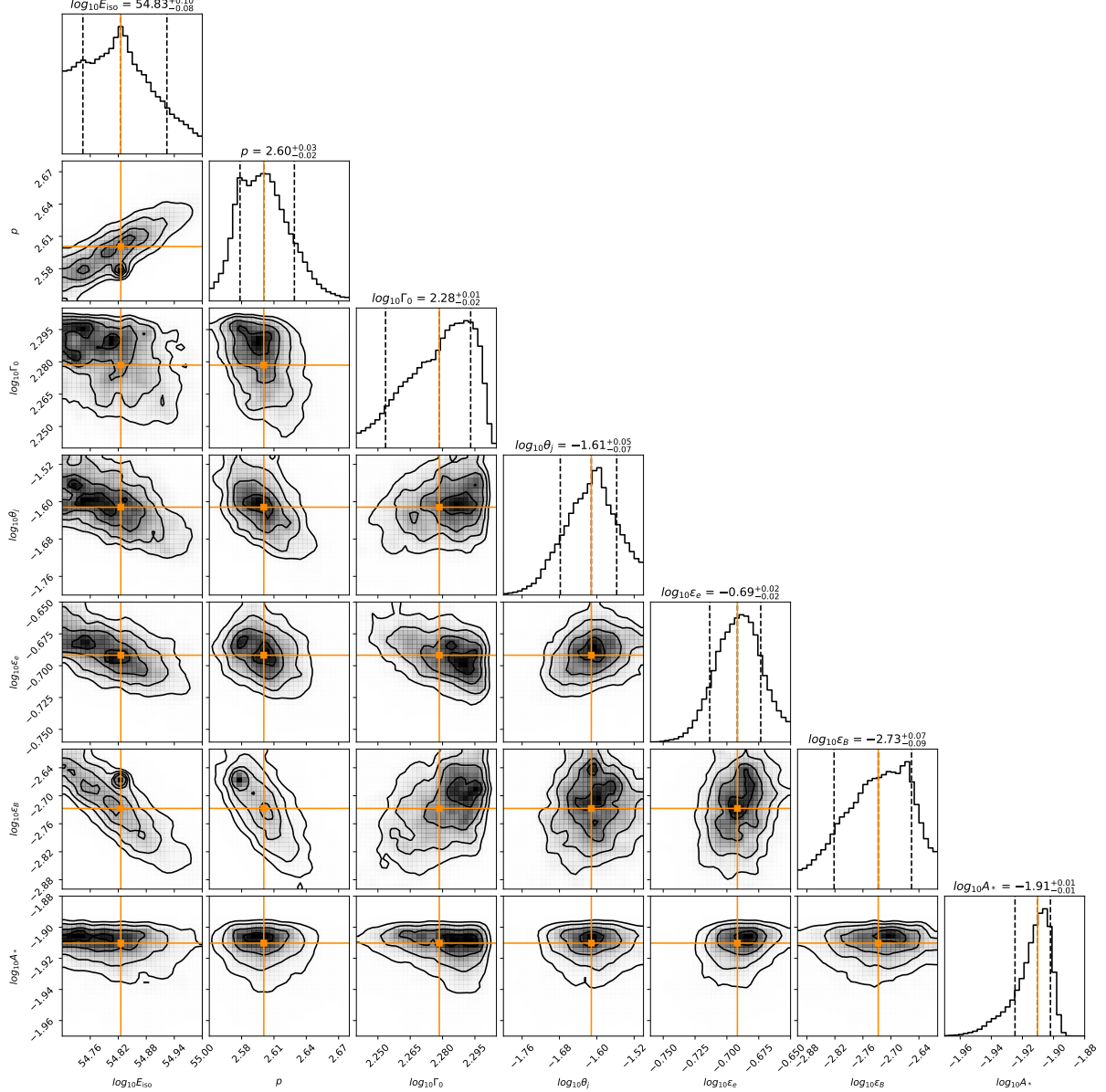


Figure 3. Contour plot for the posterior distributions of parameters.

The derived model parameters are reported in Table 1, and their posterior distributions are shown in Figures 3.

It shows that the initial $\sim T_0 + 400$ s GeV emission observed by *Fermi*/LAT in Figure 2 may be dominated by the prompt emission. Only the long lasting emission in the time range from $T_0 + 3000$ s to $T_0 + 20000$ s can be well explained by the external-forward shock radiation from the jet only. Obviously, our model explains the early time radio-to-GeV band data well. The model light curves in radio bands are consistent with the re-

ported observations¹⁰. It is worth noting that the excess of the model light curve to ~ 15 GHz band radio observations at early times is possibly due to the radiation from a reverse shock (de Ugarte Postigo et al. 2022a). We show the HAWC 95% upper limit on the flux at 1 TeV in Figure 2, and find that our result satisfies this constraint.

¹⁰ The latest observations in radio bands have been reported during the review of this paper. Our predicted curves are beyond the data and cannot be corrected by further fitting, which suggest more considerations. See discussion in Section 4.

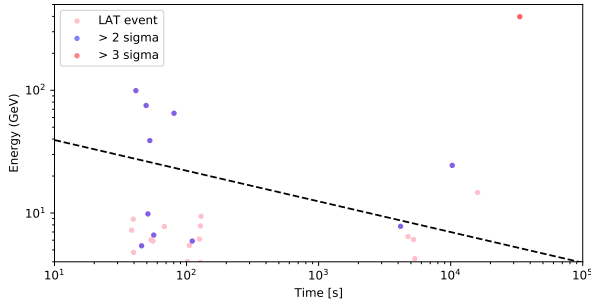


Figure 4. The red, blue, and pink dots represent photon events (> 5 GeV, within 1°) with different probabilities originating from GRB 221009A, respectively. The photon energy of the only red dot is 397.7 GeV, which is consistent with the result of Xia et al. (2022). The black dashed line is the maximum photon energy that synchrotron radiation can reach.

The jet of GRB 221009A towards us seems to propagate in a wind dominated environment with no significant density jump in the radial profile. Based on our inference result, the parameter describing the intensity of the wind $A_* = 1.2 \times 10^{-2}$, shows that the progenitor had a relatively small outflow of material prior to the burst. The microscopic physical parameters $\epsilon_e = 0.2$ and $\epsilon_B = 1.86 \times 10^{-3}$ lie within the typical value ranges. We notice that the half-opening angle of jet $\theta_j \simeq 1^\circ.4$ is mainly determined by z band data we used, which may be changed by observational data with better qualities. The combination of parameters is not exceptional, suggesting that GRB 221009A could be a typical wind environment dominated long GRB. We calculate the efficiency of prompt emission to the total energy of jet as $\eta_\gamma = E_{\gamma,\text{iso}}/(E_{\gamma,\text{iso}} + E_{\text{k},\text{iso}}) \sim 69\%$ (An et al. 2023; Yang et al. 2023) which is consistent with the expectation of the fireball model (e.g., Lloyd-Ronning & Zhang 2004; Zhang et al. 2007). Furthermore, we find that the inclusion of GeV data partly breaks the parameter degeneracy commonly observed in GRB afterglow fitting (e.g., Ren et al. 2020), underlining the significance of high-energy data in determining accurate parameters for GRB afterglows. Based on the derived model parameters, we also calculate the maximum photon energy generated by the synchrotron radiation (Cheng & Wei 1996; Fan et al. 2013), which indicates that the high-energy photons come from inverse Compton radiation by comparing the *Fermi*/LAT observations (see Figure 4).

3.3. Spectral Energy Distribution

By using the parameters of fitting results, we show the SEDs of GRB 221009A afterglow in different timeslices, see Figure 5. We show the observed spectral data and corresponding fitting curves within $T_0 + [4300, 5600]$ s for

Fermi/LAT, and $T_0 + [3453, 4643]$ s for *Swift*/XRT, respectively. We also plot the SED of $T_0 + [220, 2000]$ s as a prediction result for the LHASSO observation spectrum. One can observe that the fit between the theoretical line and the observations is quite good in the X-ray and GeV bands. Comparing the sensitivity curves of LHASSO, MAGIC, and CTA with the SED in our model, we find that the radiation in the $0.1 - 10$ TeV band is extremely bright for detections during $T_0 + [220, 2000]$ s. Our model gives the maximum SSC radiation flux around 300 GeV, with the value of $\sim 10^{-7}$ erg cm $^{-2}$ s $^{-1}$. We find that the VHE radiation of GRB 221009A has been cut off around 10 TeV as a result of EBL absorption up to the redshift $z = 0.151$ (Domínguez et al. 2011). Compared with the sensitivity curve of LHASSO, the highest energy photons from the SSC process with energy of 11 TeV can be detected by LHASSO with 2000 seconds exposure by using the EBL model of Domínguez et al. (2011). If the 18 TeV photon detected by LHASSO at $T_0 + 2000$ s was realistic, it is hard to explain by the SSC mechanism only and suggest the existence of other radiation processes. Considering that EBL absorption has a rate of $e^{-\tau_{\text{EBL}}} \sim 10^{-8}$ at 18 TeV, the intrinsic flux required to account for the radiation process of this photon event is approximately larger than 10^{-2} erg cm $^{-2}$ s $^{-1}$ for the estimated sensitivity thresholds of LHASSO. This is corresponding to the radiation luminosity greater than $\sim 6.5 \times 10^{53}$ erg s $^{-1}$ at ~ 18 TeV. Some possibilities can explain this phenomenon, such as hadronic processes (e.g., synchrotron radiation of protons, Aharonian 2000; Alves et al. 2018), Lorentz invariance violation (LIV) and Axion-like particles (e.g., Galanti et al. 2022; Nakagawa et al. 2022; Finke & Razzaque 2023; Li & Ma 2023), or the need for corrections to the EBL field of low-energy photons.

4. DISCUSSION

During the review process of this paper, several pieces of data were public. The radio afterglow of GRB 221009A exhibits a strange behavior on its spectrum, which is difficult to explain from a standard ISM or wind environment perspective (see Laskar et al. 2023, for detailed discussion). Figure 2 contains the radio data from Laskar et al. (2023) confirming that our model is inconsistent with the radio afterglow. On the other hand, the spectroscopy from JWST, HST and X-shooter shows flat NIR spectra (Levan et al. 2023; Malesani et al. 2023, where they proposed $p < 2$), again implying a violation of the standard model. Regardless, the data and analysis released so far seem to indicate that GRB 221009A exhibits a more complex radiation

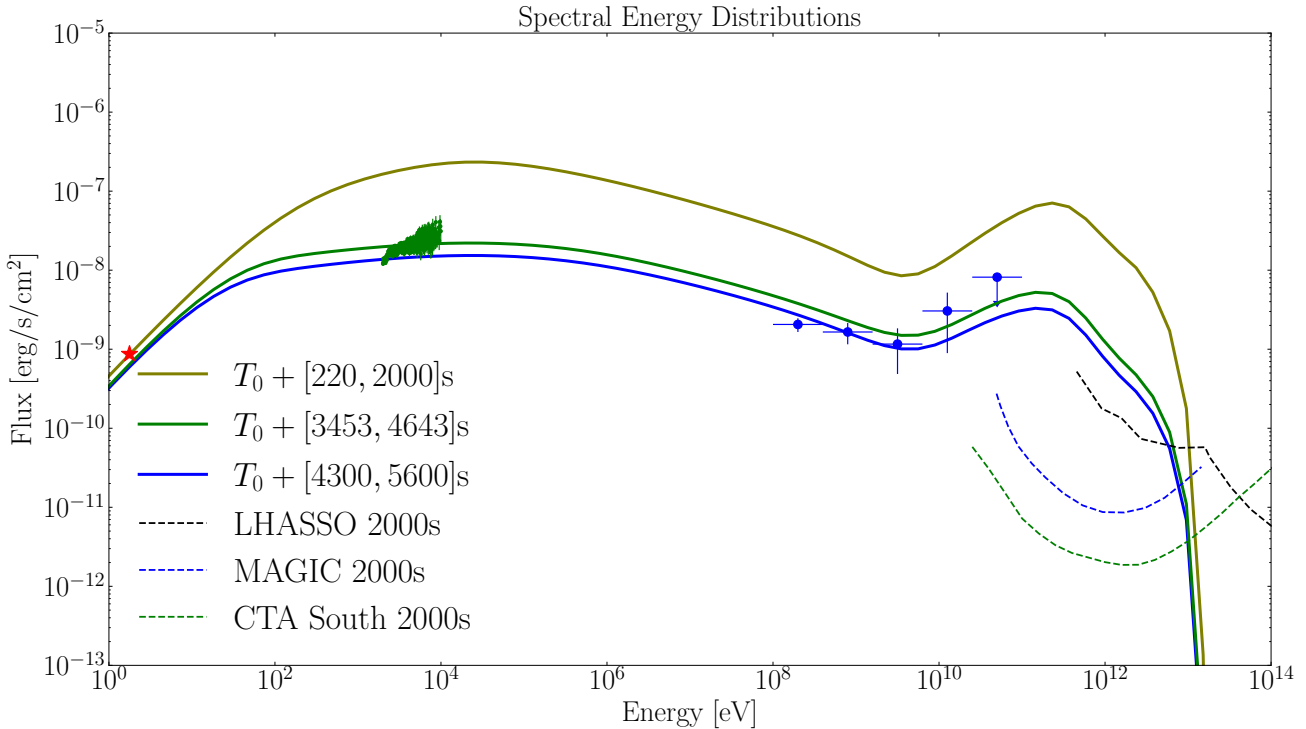


Figure 5. Afterglow SEDs of three chosen timeslices. The red star marks the R band data at $T_0 + 4150$ seconds from Belkin et al. (2022b), the green points mark the $2 - 10$ keV *Swift*/XRT data within $T_0 + [3453, 4643]$ s, and the blue points mark the $0.1 - 10$ GeV *Fermi*/LAT data within $T_0 + [4300, 5600]$ s, respectively. The black, blue, and green dashed lines correspond to the detection sensitivities of LHASSO, MAGIC, and CTA in 2000 seconds, respectively (Cao et al. 2019).

behavior than was expected based on a limited amount of information available.

The broadband afterglows of GRB 221009A have been explained in several papers using structured jet models (e.g., Sato et al. 2022; O’Connor et al. 2023). The structured jet picture has been proposed (e.g., Mészáros et al. 1998; Dai & Gou 2001; Zhang & Mészáros 2002; Rossi et al. 2002) and supported by GRB 170817A (e.g., Troja et al. 2017; Lazzati et al. 2018; Ren et al. 2020; Makhathini et al. 2021; Balasubramanian et al. 2022). Complex geometry produces the atypical spectral behaviors, but it also introduces a number of free parameters. Recent works invoking the structured jet to interpret GRB 221009A have not yet added a full fit to the multiband afterglows, which may undermine the credibility of the model. Other possible explanations imply some changes in microscopic parameters (e.g., p , ϵ_e , ϵ_B) corresponding to the shock acceleration behavior and the dissipative mechanism of energy within the shocked material that is still poorly understood (e.g., Laskar et al. 2023; Levan et al. 2023; Malesani et al. 2023).

It is possible to distinguish the correct direction of the model improvement based on the early afterglow data and future observations. Due to the high zenith Angle at the time of the burst, LHASSO was able to

record the high-energy afterglow of GRB 221009A in a highly sensitive state. This may help us to distinguish between different models. As has been pointed out, the rising slope of the early afterglow would give a strong constraint on the wind model. A typical stellar wind environment gives the early light curve that is different from the behavior predicted in an ISM environment (e.g., Wu et al. 2004, 2005; Fan et al. 2008; Zhao & Cheng 2022). However, considering the long-duration prompt emission of GRB 221009A, we want to point out the possible influence of prompt radiation on the early-time observations, for instance, the EIC processes and the internal hadronic dissipation (Zhang et al. 2022; Rudolph et al. 2023; Wang et al. 2023), and even the early energy injection (Li et al. 2023). In addition, possibly existing reverse shock may also play an important role (Kobayashi & Zhang 2003; Wu et al. 2003), but there has been no early afterglow data released yet. No matter whether a complex jet structure or a modification of the radiation process is preferred, studies on GRB 221009A will provide us with deeper insights.

5. SUMMARY & CONCLUSIONS

In this paper, we have modeled the dynamics and radiation physics of the afterglow of the brightest GRB 221009A in detail. The afterglow of GRB 221009A

can be explained by a relativistic jet with an initial Lorentz factor $\Gamma_0 \simeq 190$ propagating in an environment dominated by a stellar wind with parameter $A_\star = 1.2 \times 10^{-2}$. Due to the lack of data of early onset bump, these are reference values as current estimates. We explained the afterglow lightcurves and SEDs of GRB 221009A by using the synchrotron radiation plus the SSC mechanism. Although we have well fitted the first week radio-to-GeV band observations, the late time radio data is hardly explained under the standard external forward shock model of a top-hat jet in a stellar wind environment. According to Laskar et al. (2023), a modification to the mechanism of relativistic synchrotron radiation or an additional population of electrons will be necessary to interpret radio data under the standard model. The other explanations like structured jet models with complex geometry are also hopeful (e.g., Sato et al. 2022; O'Connor et al. 2023).

In this paper, we have presented the prediction of SSC composition under the standard stellar wind environment model as a useful reference. Our results show that the SSC component with photon energy large than 100 GeV is extremely bright during the first ~ 2000 seconds after the *Fermi*/GBM trigger time T_0 of GRB 221009A. The time integral SED within $T_0 + 220$ s to $T_0 + 2000$ s shows the SSC component has peaked in ~ 300 GeV and the peak flux $\nu F_\nu(300 \text{ GeV}) \sim 10^{-7} \text{ erg cm}^{-2} \text{ s}^{-1}$. Spectra above 300 GeV corrected with the EBL show an approximate power-law distribution up to 1 TeV, and rapidly drops with photon energies greater than 1 TeV before a cut off at approximately 10 TeV. Our results indicate that the SSC component is very promising for the interpretation of VHE emission from GRB 221009A. If the 18 TeV event detected by LHASSO is realistic, we suggest an additional component (relative to the SSC component) to account for photons beyond 10 TeV, e.g., synchrotron radiation of protons. The corresponding luminosity of such a radiation process is required to have at least $\nu L_\nu \sim 6.5 \times 10^{53} \text{ erg s}^{-1}$ at 18 TeV. Also, other possible reasons such as Lorentz invariance violation (LIV) or corrections to the EBL field needs to be examined. Furthermore, we find that the inclusion of GeV data partly breaks the parameter degeneracy commonly observed in GRB afterglow fitting (e.g., Ren et al. 2020), underlining the significance of high-energy data in determining accurate parameters for GRB afterglows.

ACKNOWLEDGMENTS

We thank the anonymous referee for the helpful comments and suggestions to improve this work. We thank D. A. Kann and T. Laskar for useful comments. This work was supported by the National Natural Science Foundation of China (grant No. 11833003). This work used data and software provided by the Fermi Science Support Center and data supplied by the UK Swift Science Data Centre at the University of Leicester. This research also used of the CTA instrument response functions provided by the CTA Consortium and Observatory, see <http://www.cta-observatory.org/science/cta-performance/> (version prod3b-v2) for more details.

Software: Matplotlib (Hunter 2007), Numpy (Harris et al. 2020), emcee (Foreman-Mackey et al. 2013), corner (Foreman-Mackey 2016), Astropy (Astropy Collaboration et al. 2013)

REFERENCES

- Abdalla, H., Adam, R., Aharonian, F., et al. 2019, Nature, 575, 464, doi: [10.1038/s41586-019-1743-9](https://doi.org/10.1038/s41586-019-1743-9)
- Acciari, V. A., Ansoldi, S., Antonelli, L. A., et al. 2021, ApJ, 908, 90, doi: [10.3847/1538-4357/abd249](https://doi.org/10.3847/1538-4357/abd249)
- Aharonian, F. A. 2000, NewA, 5, 377, doi: [10.1016/S1384-1076\(00\)00039-7](https://doi.org/10.1016/S1384-1076(00)00039-7)
- Alves, E. P., Zrake, J., & Fiuzza, F. 2018, PhRvL, 121, 245101, doi: [10.1103/PhysRevLett.121.245101](https://doi.org/10.1103/PhysRevLett.121.245101)
- An, Z.-H., Antier, S., Bi, X.-Z., et al. 2023, arXiv e-prints, arXiv:2303.01203, doi: [10.48550/arXiv.2303.01203](https://doi.org/10.48550/arXiv.2303.01203)
- Asano, K., Murase, K., & Toma, K. 2020, ApJ, 905, 105, doi: [10.3847/1538-4357/abc82c](https://doi.org/10.3847/1538-4357/abc82c)
- Astropy Collaboration, Robitaille, T. P., Tollerud, E. J., et al. 2013, A&A, 558, A33, doi: [10.1051/0004-6361/201322068](https://doi.org/10.1051/0004-6361/201322068)
- Atteia, J.-L. 2022, GRB Coordinates Network, 32793, 1
- Atwood, W., Abdo, A. A., Ackermann, M., et al. 2009, The Astrophysical Journal, 697, 1071
- Balasubramanian, A., Corsi, A., Mooley, K. P., et al. 2022, ApJ, 938, 12, doi: [10.3847/1538-4357/ac9133](https://doi.org/10.3847/1538-4357/ac9133)
- Belkin, S., Nazarov, S., Pozanenko, A., & Pankov, N. 2022a, GRB Coordinates Network, 32684, 1
- Belkin, S., Pozanenko, A., E., K., & et al. 2022b, GRB Coordinates Network, 32645, 1
- Bikmaev, I., Khamitov, I., Irtuganov, E., et al. 2022a, GRB Coordinates Network, 32743, 1
- . 2022b, GRB Coordinates Network, 32752, 1
- Bissaldi, E., Omodei, N., Kerr, M., & et al. 2022a, GRB Coordinates Network, 32637, 1
- . 2022b, GRB Coordinates Network, 32637, 1
- Brethauer, D., Grefenstette, B., Racusin, J., et al. 2022, The Astronomer's Telegram, 15665, 1
- Bright, J., Rhodes, L., R., F., & et al. 2022, GRB Coordinates Network, 32653, 1
- Brivio, R., D'Avanzo, P., Fugazza, D., Melandri, A., & Covino, S. 2022, GRB Coordinates Network, 32652, 1
- Burns, E., Svinkin, D., Fenimore, E., et al. 2023, arXiv e-prints, arXiv:2302.14037, doi: [10.48550/arXiv.2302.14037](https://doi.org/10.48550/arXiv.2302.14037)
- Cao, Z., della Volpe, D., Liu, S., et al. 2019, arXiv e-prints, arXiv:1905.02773. <https://arxiv.org/abs/1905.02773>
- Castro-Tirado, A. J., Sanchez-Ramirez, R., Hu, Y.-D., & et al. 2022, GRB Coordinates Network, 32686, 1
- Chen, T.-W., Pan, Y.-C., Hsiao, H.-Y., Lin, C.-S., & Guo, J.-K. 2022, GRB Coordinates Network, 32667, 1
- Cheng, K., & Wei, D. 1996, Monthly Notices of the Royal Astronomical Society, 283, L133
- Chevalier, R. A., & Li, Z.-Y. 2000, ApJ, 536, 195, doi: [10.1086/308914](https://doi.org/10.1086/308914)
- Dai, Z. G., & Gou, L. J. 2001, ApJ, 552, 72, doi: [10.1086/320463](https://doi.org/10.1086/320463)
- Dai, Z. G., & Lu, T. 1998, MNRAS, 298, 87, doi: [10.1046/j.1365-8711.1998.01681.x](https://doi.org/10.1046/j.1365-8711.1998.01681.x)
- de Ugarte Postigo, A., Bremer, M., Thoene, C. C., & et al. 2022a, GRB Coordinates Network, 32676, 1
- de Ugarte Postigo, A., Izzo, L., Pugliese, G., & et al. 2022b, GRB Coordinates Network, 32648, 1
- de Wet, S., & Groot, P. 2022, GRB Coordinates Network, 32646, 1
- Dermer, C. D., Chiang, J., & Mitman, K. E. 2000, ApJ, 537, 785, doi: [10.1086/309061](https://doi.org/10.1086/309061)
- Dichiara, S., Groppi, J. D., Kennea, J. A., & Kuin, N. P. M. 2022, GRB Coordinates Network, 32632, 1
- Domínguez, A., Primack, J. R., Rosario, D. J., et al. 2011, MNRAS, 410, 2556, doi: [10.1111/j.1365-2966.2010.17631.x](https://doi.org/10.1111/j.1365-2966.2010.17631.x)
- Evans, P., Beardmore, A. P., Page, K. L., et al. 2007, Astronomy & Astrophysics, 469, 379
- Evans, P., Beardmore, A., Page, K., et al. 2009, Monthly Notices of the Royal Astronomical Society, 397, 1177
- Fan, Y. Z., & Piran, T. 2006, MNRAS, 369, 197, doi: [10.1111/j.1365-2966.2006.10280.x](https://doi.org/10.1111/j.1365-2966.2006.10280.x)
- Fan, Y. Z., Piran, T., Narayan, R., & Wei, D.-M. 2008, MNRAS, 384, 1483, doi: [10.1111/j.1365-2966.2007.12765.x](https://doi.org/10.1111/j.1365-2966.2007.12765.x)
- Fan, Y.-Z., Tam, P., Zhang, F.-W., et al. 2013, The Astrophysical Journal, 776, 95
- Farah, W., Bright, J., A., P., & et al. 2022, GRB Coordinates Network, 32655, 1
- Finke, J. D., & Razzaque, S. 2023, ApJL, 942, L21, doi: [10.3847/2041-8213/acade1](https://doi.org/10.3847/2041-8213/acade1)
- Finke, J. D., Razzaque, S., & Dermer, C. D. 2010, ApJ, 712, 238, doi: [10.1088/0004-637X/712/1/238](https://doi.org/10.1088/0004-637X/712/1/238)
- Foreman-Mackey, D. 2016, The Journal of Open Source Software, 1, 24, doi: [10.21105/joss.00024](https://doi.org/10.21105/joss.00024)
- Foreman-Mackey, D., Hogg, D. W., Lang, D., & Goodman, J. 2013, PASP, 125, 306, doi: [10.1086/670067](https://doi.org/10.1086/670067)
- Fukami, S., Berti, A., Loporchio, S., et al. 2021, in Proceedings of 37th International Cosmic Ray Conference — PoS(ICRC2021), Vol. 395, 788, doi: [10.22323/1.395.0788](https://doi.org/10.22323/1.395.0788)
- Galanti, G., Roncadelli, M., & Tavecchio, F. 2022, arXiv e-prints, arXiv:2211.06935, doi: [10.48550/arXiv.2211.06935](https://doi.org/10.48550/arXiv.2211.06935)
- Geng, J.-J., Huang, Y.-F., Wu, X.-F., Zhang, B., & Zong, H.-S. 2018, ApJS, 234, 3, doi: [10.3847/1538-4365/aa9e84](https://doi.org/10.3847/1538-4365/aa9e84)
- Gould, R. J., & Schréder, G. P. 1967, Physical Review, 155, 1408, doi: [10.1103/PhysRev.155.1408](https://doi.org/10.1103/PhysRev.155.1408)

- Gregory, S. P., Myungshin, I., Yuji, U., & Hyun-I, S. 2022, GRB Coordinates Network, 32659, 1
- Groot, P., Vreeswijk, P., Ter Horst, R., et al. 2022, GRB Coordinates Network, 32678, 1
- H. E. S. S. Collaboration, Abdalla, H., Aharonian, F., et al. 2021, Science, 372, 1081, doi: [10.1126/science.abe8560](https://doi.org/10.1126/science.abe8560)
- Harris, C. R., Millman, K. J., van der Walt, S. J., et al. 2020, Nature, 585, 357, doi: [10.1038/s41586-020-2649-2](https://doi.org/10.1038/s41586-020-2649-2)
- HAWC collaboration. 2022, GRB Coordinates Network, 32683, 1
- He, H.-N., Wang, X.-Y., Yu, Y.-W., & Mészáros, P. 2009, ApJ, 706, 1152, doi: [10.1088/0004-637x/706/2/1152](https://doi.org/10.1088/0004-637x/706/2/1152)
- Hu, Y.-D., Casanova, V., Fernandez-Garcia, E., & Castro-Tirado, M. A. 2022, GRB Coordinates Network, 32644, 1
- Huang, Y. 2022, ApJ, 931, 150, doi: [10.3847/1538-4357/ac6d52](https://doi.org/10.3847/1538-4357/ac6d52)
- Huang, Y., Hu, S.-C., Chen, S.-Z., & et al. 2022, GRB Coordinates Network, 32677, 1
- Huber, M., Schultz, A., Chambers, K., et al. 2022, GRB Coordinates Network, 32758, 1
- Hunter, J. D. 2007, Computing in Science and Engineering, 9, 90, doi: [10.1109/MCSE.2007.55](https://doi.org/10.1109/MCSE.2007.55)
- Hurley, K., Dingus, B. L., Mukherjee, R., et al. 1994, Nature, 372, 652, doi: [10.1038/372652a0](https://doi.org/10.1038/372652a0)
- Jiang, G.-S., & Shu, C.-W. 1996, Journal of Computational Physics, 126, 202, doi: [10.1006/jcph.1996.0130](https://doi.org/10.1006/jcph.1996.0130)
- Joshi, J. C., & Razzaque, S. 2021, MNRAS, 505, 1718, doi: [10.1093/mnras/stab1329](https://doi.org/10.1093/mnras/stab1329)
- Joshi, J. C., & Razzaque, S. 2021, MNRAS, 505, 1718, doi: [10.1093/mnras/stab1329](https://doi.org/10.1093/mnras/stab1329)
- Kann, D. A., Agayeva, S., Aivazyan, V., et al. 2023, arXiv e-prints, arXiv:2302.06225, doi: [10.48550/arXiv.2302.06225](https://doi.org/10.48550/arXiv.2302.06225)
- Kim, V., Krugov, M., Pozanenko, A., et al. 2022, GRB Coordinates Network, 32670, 1
- Kobayashi, S., & Zhang, B. 2003, ApJ, 597, 455, doi: [10.1086/378283](https://doi.org/10.1086/378283)
- Kumar, H., Swain, V., Waratkar, G., et al. 2022, GRB Coordinates Network, 32662, 1
- Kumar, P., Hernández, R. A., Bošnjak, Ž., & Barniol Duran, R. 2012, MNRAS, 427, L40, doi: [10.1111/j.1745-3933.2012.01341.x](https://doi.org/10.1111/j.1745-3933.2012.01341.x)
- Laskar, T., Alexander, K. D., Ayache, E., & et al. 2022, GRB Coordinates Network, 32740, 1
- Laskar, T., Alexander, K. D., Margutti, R., et al. 2023, arXiv e-prints, arXiv:2302.04388, doi: [10.48550/arXiv.2302.04388](https://doi.org/10.48550/arXiv.2302.04388)
- Lazzati, D., Perna, R., Morsony, B. J., et al. 2018, PhRvL, 120, 241103, doi: [10.1103/PhysRevLett.120.241103](https://doi.org/10.1103/PhysRevLett.120.241103)
- Levan, A. J., Lamb, G. P., Schneider, B., et al. 2023, arXiv e-prints, arXiv:2302.07761, doi: [10.48550/arXiv.2302.07761](https://doi.org/10.48550/arXiv.2302.07761)
- Li, H., & Ma, B.-Q. 2023, Astroparticle Physics, 148, 102831, doi: [10.1016/j.astropartphys.2023.102831](https://doi.org/10.1016/j.astropartphys.2023.102831)
- Li, J., Lin, D.-B., Lu, R.-J., et al. 2023, ApJ, 944, 21, doi: [10.3847/1538-4357/acaf68](https://doi.org/10.3847/1538-4357/acaf68)
- Lloyd-Ronning, N. M., & Zhang, B. 2004, ApJ, 613, 477, doi: [10.1086/423026](https://doi.org/10.1086/423026)
- MAGIC Collaboration, Acciari, V. A., Ansoldi, S., et al. 2019, Nature, 575, 459, doi: [10.1038/s41586-019-1754-6](https://doi.org/10.1038/s41586-019-1754-6)
- Makhathini, S., Mooley, K. P., Brightman, M., et al. 2021, ApJ, 922, 154, doi: [10.3847/1538-4357/ac1ffc](https://doi.org/10.3847/1538-4357/ac1ffc)
- Malesani, D. B., Levan, A. J., Izzo, L., et al. 2023, arXiv e-prints, arXiv:2302.07891, doi: [10.48550/arXiv.2302.07891](https://doi.org/10.48550/arXiv.2302.07891)
- Mészáros, P., Rees, M. J., & Wijers, R. A. M. J. 1998, ApJ, 499, 301, doi: [10.1086/305635](https://doi.org/10.1086/305635)
- Murase, K., Ioka, K., Nagataki, S., & Nakamura, T. 2006, ApJL, 651, L5, doi: [10.1086/509323](https://doi.org/10.1086/509323)
- Murase, K., Toma, K., Yamazaki, R., & Mészáros, P. 2011, ApJ, 732, 77, doi: [10.1088/0004-637x/732/2/77](https://doi.org/10.1088/0004-637x/732/2/77)
- Nakagawa, S., Takahashi, F., Yamada, M., & Yin, W. 2022, arXiv e-prints, arXiv:2210.10022, doi: [10.48550/arXiv.2210.10022](https://doi.org/10.48550/arXiv.2210.10022)
- Nakar, E., Ando, S., & Sari, R. 2009, ApJ, 703, 675, doi: [10.1088/0004-637X/703/1/675](https://doi.org/10.1088/0004-637X/703/1/675)
- Nava, L., Sironi, L., Ghisellini, G., Celotti, A., & Ghirlanda, G. 2013, MNRAS, 433, 2107, doi: [10.1093/mnras/stt872](https://doi.org/10.1093/mnras/stt872)
- O'Connor, B., Troja, E., Ryan, G., et al. 2023, arXiv e-prints, arXiv:2302.07906, doi: [10.48550/arXiv.2302.07906](https://doi.org/10.48550/arXiv.2302.07906)
- Omodei, N., Bruel, P., Bregeon, J., et al. 2022, GRB Coordinates Network, 32760, 1
- Pe'er, A. 2012, ApJL, 752, 8, doi: [10.1088/2041-8205/752/1/L8](https://doi.org/10.1088/2041-8205/752/1/L8)
- Pei, Y. C. 1992, ApJ, 395, 130, doi: [10.1086/171637](https://doi.org/10.1086/171637)
- Pillera, R., Bissaldi, E., Omodei, N., La Mura, G., & Longo, F. 2022, GRB Coordinates Network, 32658, 1
- Planck Collaboration, Ade, P. A. R., Aghanim, N., et al. 2016, A&A, 594, A13, doi: [10.1051/0004-6361/201525830](https://doi.org/10.1051/0004-6361/201525830)
- Ren, J., Lin, D.-B., Zhang, L.-L., et al. 2020, ApJ, 901, L26, doi: [10.3847/2041-8213/abb672](https://doi.org/10.3847/2041-8213/abb672)
- Rhodes, L., Bright, J., Fender, R., & et al. 2022, GRB Coordinates Network, 32700, 1
- Rossi, E., Lazzati, D., & Rees, M. J. 2002, MNRAS, 332, 945, doi: [10.1046/j.1365-8711.2002.05363.x](https://doi.org/10.1046/j.1365-8711.2002.05363.x)
- Rudolph, A., Petropoulou, M., Winter, W., & Bošnjak, Ž. 2023, ApJL, 944, L34, doi: [10.3847/2041-8213/acb6d7](https://doi.org/10.3847/2041-8213/acb6d7)

- Sahu, S., Valadez Polanco, I. A., & Rajpoot, S. 2022, ApJ, 929, 70, doi: [10.3847/1538-4357/ac5cc6](https://doi.org/10.3847/1538-4357/ac5cc6)
- Sari, R., & Esin, A. A. 2001, ApJ, 548, 787, doi: [10.1086/319003](https://doi.org/10.1086/319003)
- Sari, R., & Piran, T. 1999, ApJL, 517, L109, doi: [10.1086/312039](https://doi.org/10.1086/312039)
- Sari, R., Piran, T., & Narayan, R. 1998, ApJ, 497, L17, doi: [10.1086/311269](https://doi.org/10.1086/311269)
- Sato, Y., Murase, K., Ohira, Y., & Yamazaki, R. 2022, arXiv e-prints, arXiv:2212.09266, doi: [10.48550/arXiv.2212.09266](https://doi.org/10.48550/arXiv.2212.09266)
- Schlafly, E. F., & Finkbeiner, D. P. 2011, ApJ, 737, 103, doi: [10.1088/0004-637X/737/2/103](https://doi.org/10.1088/0004-637X/737/2/103)
- Shrestha, M., Bostroem, K., Sand, D., Alexander, K. D., & et al. 2022a, GRB Coordinates Network, 32771, 1
- Shrestha, M., Sand, D., Alexander, K., et al. 2022b, GRB Coordinates Network, 32759, 1
- Strausbaugh, S., & Cucchiara, A. 2022, GRB Coordinates Network, 32693, 1
- Suda, Y., Artero, M., Asano, K., et al. 2021, in Proceedings of 37th International Cosmic Ray Conference — PoS(ICRC2021), Vol. 395, 797, doi: [10.22323/1.395.0797](https://doi.org/10.22323/1.395.0797)
- Troja, E., Piro, L., van Eerten, H., et al. 2017, Nature, 551, 71, doi: [10.1038/nature24290](https://doi.org/10.1038/nature24290)
- Trushkin, S. A., Nizhelskij, N. N., Tsybulev, P. G., & Erkenov, A. K. 2022, The Astronomer's Telegram, 15671, 1
- Urata, Y., Huang, K. Y., Covino, S., & et al. 2022, GRB Coordinates Network, 32761, 1
- Veres, P., Burns, E., Bissaldi, E., Lesage, S., & Roberts, o. 2022, GRB Coordinates Network, 32636, 1
- Vinko, J., Bodl, A., Pal, A., et al. 2022, GRB Coordinates Network, 32709, 1
- Wang, K., Ma, Z.-P., Liu, R.-Y., et al. 2023, arXiv e-prints, arXiv:2302.11111, doi: [10.48550/arXiv.2302.11111](https://doi.org/10.48550/arXiv.2302.11111)
- Wang, X.-Y., Liu, R.-Y., Zhang, H.-M., Xi, S.-Q., & Zhang, B. 2019, ApJ, 884, 117, doi: [10.3847/1538-4357/ab426c](https://doi.org/10.3847/1538-4357/ab426c)
- Watson, A., Butler, N., Dichiara, S., et al. 2022, GRB Coordinates Network, 32692, 1
- Waxman, E. 1997, ApJL, 485, L5, doi: [10.1086/310809](https://doi.org/10.1086/310809)
- Williams, M. A., Kennea, J. A., Dichiara, S., et al. 2023, arXiv e-prints, arXiv:2302.03642, doi: [10.48550/arXiv.2302.03642](https://doi.org/10.48550/arXiv.2302.03642)
- Wu, X. F., Dai, Z. G., Huang, Y. F., & Lu, T. 2003, MNRAS, 342, 1131, doi: [10.1046/j.1365-8711.2003.06602.x](https://doi.org/10.1046/j.1365-8711.2003.06602.x)
- . 2005, ApJ, 619, 968, doi: [10.1086/426666](https://doi.org/10.1086/426666)
- Wu, X. F., Dai, Z. G., Huang, Y. F., & Ma, H. T. 2004, ChJAA&A, 4, 455, doi: [10.1088/1009-9271/4/5/455](https://doi.org/10.1088/1009-9271/4/5/455)
- Xia, Z.-Q., Wang, Y., Yuan, Q., & Fan, Y.-Z. 2022, GRB Coordinates Network, 32748, 1
- Xue, R., Tam, P., Wagner, S., et al. 2009, The Astrophysical Journal, 703, 60
- Yamasaki, S., & Piran, T. 2022, MNRAS, 512, 2142, doi: [10.1093/mnras/stac483](https://doi.org/10.1093/mnras/stac483)
- Yang, J., Zhao, X.-H., Yan, Z., et al. 2023, arXiv e-prints, arXiv:2303.00898, doi: [10.48550/arXiv.2303.00898](https://doi.org/10.48550/arXiv.2303.00898)
- Zaznabin, I., Burenin, R., & Eselevich, M. 2022, GRB Coordinates Network, 32729, 1
- Zhang, B. 2018, The Physics of Gamma-Ray Bursts, doi: [10.1017/9781139226530](https://doi.org/10.1017/9781139226530)
- Zhang, B., & Mészáros, P. 2001, ApJ, 559, 110, doi: [10.1086/322400](https://doi.org/10.1086/322400)
- . 2002, ApJ, 571, 876, doi: [10.1086/339981](https://doi.org/10.1086/339981)
- Zhang, B., Liang, E., Page, K. L., et al. 2007, ApJ, 655, 989, doi: [10.1086/510110](https://doi.org/10.1086/510110)
- Zhang, B. T., Murase, K., Ioka, K., et al. 2022, arXiv e-prints, arXiv:2211.05754, doi: [10.48550/arXiv.2211.05754](https://doi.org/10.48550/arXiv.2211.05754)
- Zhang, B. T., Murase, K., Yuan, C., Kimura, S. S., & Mészáros, P. 2021, ApJL, 908, L36, doi: [10.3847/2041-8213/abe0b0](https://doi.org/10.3847/2041-8213/abe0b0)
- Zhang, H., Christie, I. M., Petropoulou, M., Rueda-Becerril, J. M., & Giannios, D. 2020, MNRAS, 496, 974, doi: [10.1093/mnras/staa1583](https://doi.org/10.1093/mnras/staa1583)
- Zhang, L.-L., Ren, J., Huang, X.-L., et al. 2021, ApJ, 917, 95, doi: [10.3847/1538-4357/ac0c7f](https://doi.org/10.3847/1538-4357/ac0c7f)
- Zhao, X.-H., & Cheng, K.-F. 2022, Universe, 8, 588, doi: [10.3390/universe8110588](https://doi.org/10.3390/universe8110588)
- Zheng, E., Zheng, W.-K., & Filippenko, A. V. 2022, GRB Coordinates Network, 32669, 1